Draft version February 5, 2008
Preprint typeset using LaTeX style emulateapj v. 04/03/99

UNTANGLING THE X-RAY EMISSION FROM THE SA GALAXY NGC 1291 WITH *CHANDRA*

Jimmy A. Irwin[1,2], Craig L. Sarazin[3], and Joel N. Bregman[1]

Draft version February 5, 2008

ABSTRACT

We present a *Chandra* ACIS-S observation of the nearby bulge-dominated Sa galaxy NGC 1291. The X-ray emission from the bulge resembles the X-ray emission from a sub-class of elliptical and S0 galaxies with low X-ray–to–optical luminosity ratios. The X-ray emission is composed of a central point-like nucleus, ∼50 point sources that are most likely low mass X-ray binaries (LMXBs), and diffuse gas detectable out to a radius of 120″ (5.2 kpc). The diffuse gas has a global temperature of $0.32^{+0.04}_{-0.03}$ keV and metallicity of 0.06 ± 0.02 solar, and both quantities marginally decrease with increasing radius. The hot gas fills the hole in the H I distribution, and the softening of the spectrum of the X-ray gas with radius might indicate a thermal coupling of the hot and cold phases of the interstellar medium as previously suggested. The integrated X-ray luminosity of the LMXBs, once normalized by the optical luminosity, is a factor of 1.4 less than in the elliptical galaxy NGC 4697 or S0 galaxy NGC 1553. The difference in $L_{X,stellar}/L_B$ between the galaxies appears to be because of a lack of very bright sources in NGC 1291. No sources above 3×10^{38} ergs s^{-1} were found in NGC 1291 when ∼7 were expected from scaling from NGC 4697 and NGC 1553. The cumulative $L_{X,stellar}/L_B$ value including only sources below 1.0×10^{38} ergs s^{-1} is remarkably similar between NGC 1291 and NGC 4697, if a recent surface brightness fluctuation-determined distance is assumed for NGC 4697. If this is a common feature of the LMXB population in early-type systems, it might be used as a distance indicator. Finally, a bright, variable ($1.6 - 3.1 \times 10^{39}$ ergs s^{-1}) source was detected at the optical center of the galaxy. Its spectrum shows excess soft emission superimposed on a highly absorbed power law component, similar to what has been found in several other low luminosity active galactic nuclei. However, the soft component does not vary in intensity like the hard component, indicating that the soft component is not reprocessed hard component emission.

Subject headings: binaries: close — galaxies: ISM — X-rays: galaxies — X-rays: ISM — X-rays: stars

1. INTRODUCTION

From a stellar population point of view, the large bulges of Sa galaxies closely resemble elliptical galaxies. It is therefore natural to ask if this similarity extends into the X-ray regime. With the launch of *Chandra*, our view of the X-ray emission from elliptical galaxies has become considerably clearer. The nature of the X-ray emission from X-ray bright (high X-ray–to–optical luminosity ratio, L_X/L_B) elliptical galaxies had been known since the days of the *Einstein Observatory* to be primarily from hot 10^7 K gas (e.g., Forman, Jones, & Tucker 1985; Trinchieri, Fabbiano, & Canizares 1986), with a small percentage of the flux from a harder component (presumably the integrated emission from a collection of low-mass X-ray binaries, hereafter LMXBs; Matsumoto et al. 1997). However, only *Chandra's* 0.″5 spatial resolution was able to resolve the X-ray emission from X-ray faint (low L_X/L_B) elliptical and S0 galaxies into its constituent parts. In the X-ray faint elliptical galaxy NGC 4697 *Chandra* found that a majority of the X-ray emission emanated from a collection of point sources, primarily LMXBs, with the remaining X-ray emission from a lower temperature diffuse interstellar medium (Sarazin, Irwin, & Bregman 2000; hereafter SIB00). In these galaxies, much of the hot interstellar medium has apparently been removed, leaving behind the X-ray binaries as the primary X-ray emission mechanism.

Whether spiral bulges more closely resemble the gas-rich X-ray bright elliptical galaxies or the stellar-dominated X-ray faint galaxies remains undetermined. Previous work with *Einstein* indicated that the average X-ray temperature of Sa galaxies was intermediate between elliptical galaxies and later-type spiral galaxies (Kim, Fabbiano, & Trinchieri 1992). Further comparisons with *ROSAT* revealed that the bulges of the two optically brightest Sa galaxies (NGC 1291 and NGC 3623) and the bulge of M31 had similar L_X/L_B values and X-ray colors as X-ray faint elliptical galaxies (Irwin & Sarazin 1998a,b). Recent *ROSAT* HRI observations of NGC 1291 found that the radial surface brightness distribution of the X-rays followed a de Vaucouleurs profile suggesting that stellar X-ray sources were responsible for the observed X-ray emission (Hogg et al. 2001), although *ROSAT* PSPC data indicated that X-ray spectrum softened with increasing radius, which would not be expected from a purely stellar component (Bregman, Hogg, & Roberts 1995). But whether the X-ray emission from spiral bulges is dominated by a stellar component can only be confirmed using the excellent spatial resolution of *Chandra*. Here, we present a *Chandra* observation of the nearby Sa galaxy NGC 1291 to resolve the question of the X-ray emission in spiral galaxies with large bulges.

[1]Department of Astronomy, University of Michigan, Ann Arbor, MI 48109-1090 E-mail: jirwin@astro.lsa.umich.edu, jbregman@umich.edu
[2]Chandra Fellow.
[3]Department of Astronomy, University of Virginia, P.O. Box 3818, Charlottesville, VA 22903-0818; E-mail: sarazin@virginia.edu

2. TARGET AND DATA REDUCTION

NGC 1291 is the optically brightest Sa galaxy in the Revised Shapley Ames Catalog with a corrected apparent magnitude of $B_0 = 9.17$. Detailed optical imaging by de Vaucouleurs (1975) revealed a central lens surrounded by a large outer ring from which two faint spiral arms emanate. Sometimes classified as a transitional SB(s)0/Sa galaxy, there are no other optically bright galaxies in velocity space near NGC 1291, although recently a large concentration of faint low surface brightness galaxies have been found around NGC 1291 (Kambas et al. 2000). The distance to NGC 1291 is uncertain, and literature values range from 6.9 Mpc to 13.8 Mpc. de Vaucouleurs (1975) gives a distance of 8.9 Mpc by assuming that the brightest stars in the weak spiral arms of NGC 1291 have an absolute magnitude of $M_B = -9.5$, and this is the distance we have assumed for this work. The corrected galactocentric velocity is 674 km s^{-1} (de Vaucouleurs 1975). At a distance of 8.9 Mpc, $1'$ corresponds to 2.6 kpc.

In this paper, we will concentrate on X-ray sources and diffuse emission seen in projection within the optical bulge of NGC 1291. We will define the bulge to be the region within an ellipse centered on the optical nucleus, with major and minor axes of $4\farcm5$ and $3\farcm7$, respectively, and at a position angle of 170° (de Vaucouleurs 1975).

NGC 1291 was observed with the Advanced CCD Imaging Spectrometer (ACIS) onboard *Chandra* at two epochs, on 2000 June 27–28, and again on 2000 November 7. The first observation (hereafter OB1) was awarded to us in AO-1 of *Chandra*, while the second observation

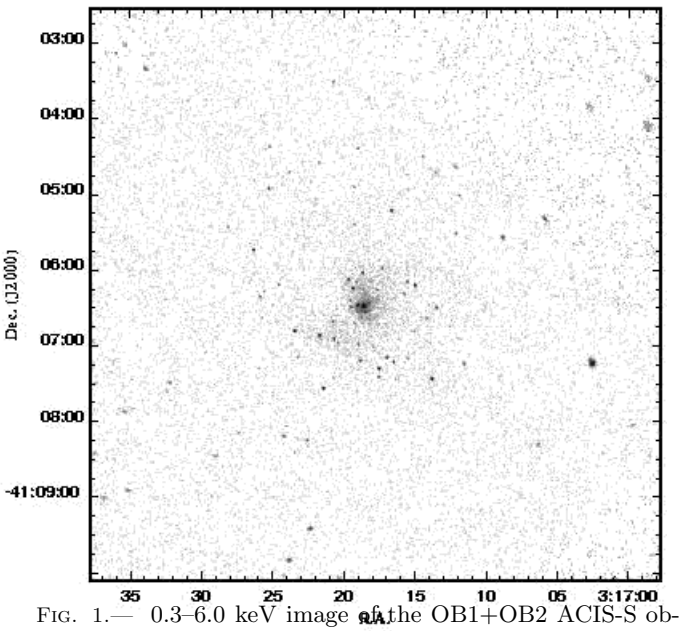

FIG. 1.— 0.3–6.0 keV image of the OB1+OB2 ACIS-S observation of NGC 1291. The image has been smoothed with a Gaussian of width $0\farcs5$ to bring out point sources and diffuse emission.

(hereafter OB2) was graciously donated to the *Chandra* archive early by Andrea Prestwich. OB1 contained one small background flare, while over a third of OB2 was taken during times of high background. The total usable exposure for OB1 and OB2 was 37,409 seconds and 23,016 seconds, respectively. Both OB1 and OB2 were taken when the focal plane temperature was –120° C. The observations were combined for the spatial analysis, and treated separately for the spectral analysis. We present data only from the backside-illuminated S3 chip. Exposure maps were generated to correct the images for vignetting. An exposure map appropriate for an energy of 0.75 keV was generated for soft energy images, while an exposure map appropriate for an energy of 3 keV was created for hard energy images. The newest spectral responses available (acisD2000-01-29fef_piN0002.fits) were used in the spectral analysis.

3. SPATIAL ANALYSIS

3.1. *X-ray Images*

The 0.3–6 keV *Chandra* image of the merged OB1+OB2 observation is shown in Figure 1. It was found that omitting energy channels above 6.0 keV reduced the background by 51% while decreasing the source emission by only 4%. The image has been lightly smoothed

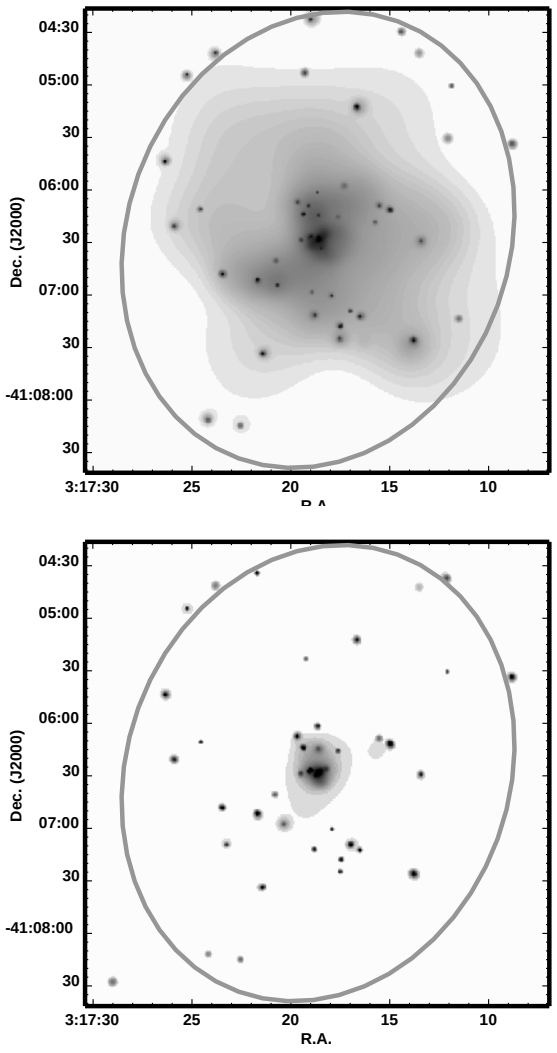

FIG. 2.— Inner $4\farcm5 \times 4\farcm5$ of NGC 1291 in the (*a*) 0.3-1.0 keV (*upper*) and (*b*) 1.5-6.0 keV (*lower*) energy band. The images have been adaptively smoothed to a minimum signal–to–noise ratio of three per smoothing beam. The ellipse represents the optical extent of the bulge as determined by de Vaucouleurs (1975).

with a Gaussian with a width of one pixel to bring out

TABLE 1
DISCRETE X-RAY SOURCES IN BULGE

Src. No.. (1)	Name (2)	R.A. (h:m:s) (3)	Dec. (°:′:″) (4)	d (arcsec) (5)	Count Rate (10^{-4} s^{-1}) (6)	SNR (7)	L_X (0.3-10 keV) (10^{37} ergs s^{-1}) (8)
1	CXOU J031718.6-410628	3:17:18.60	−41:06:28.3	0.00	255.25±9.09	28.09	305.20
2	CXOU J031718.7-410630	3:17:18.79	−41:06:30.2	2.86	19.67±2.52	7.80	13.39
3	CXOU J031718.9-410627	3:17:18.98	−41:06:27.0	4.52	25.50±2.87	8.88	17.36
4	CXOU J031718.2-410626	3:17:18.22	−41:06:26.4	4.70	8.96± 1.70	5.26	6.10
5	CXOU J031718.4-410633	3:17:18.48	−41:06:33.4	5.21	11.49±1.93	5.96	7.82
6	CXOU J031719.1-410628	3:17:19.12	−41:06:28.1	5.92	19.71±2.53	7.81	13.42
7	CXOU J031718.7-410637	3:17:18.75	−41:06:37.3	9.12	5.33±1.31	4.06	3.63
8	CXOU J031719.4-410629	3:17:19.47	−41:06:29.1	9.95	6.69±1.47	4.55	4.56
9	CXOU J031719.5-410623	3:17:19.55	−41:06:24.0	11.57	5.62±1.35	4.17	3.83
10	CXOU J031718.6-410615	3:17:18.63	−41:06:15.1	13.22	8.23±1.63	5.05	5.61
11	CXOU J031719.2-410641	3:17:19.28	−41:06:41.9	15.63	4.49±1.20	3.73	3.06
12	CXOU J031717.6-410615	3:17:17.65	−41:06:15.9	16.38	7.61±1.57	4.85	5.18
13	CXOU J031719.3-410614	3:17:19.37	−41:06:14.4	16.42	34.04±3.32	10.26	23.18
14	CXOU J031719.1-410609	3:17:19.13	−41:06:09.4	19.84	4.89±1.26	3.89	3.33
15	CXOU J031719.6-410607	3:17:19.68	−41:06:07.7	23.96	12.21±1.99	6.14	8.31
16	CXOU J031718.6-410602	3:17:18.66	−41:06:02.2	26.08	9.76±1.78	5.49	6.64
17	CXOU J031720.7-410641	3:17:20.79	−41:06:41.0	27.85	4.54±1.21	3.75	3.09
18	CXOU J031718.9-410658	3:17:18.96	−41:06:58.7	30.67	3.26±1.03	3.18	2.22
19	CXOU J031717.9-410700	3:17:17.95	−41:07:00.7	33.22	8.33±1.64	5.08	5.67
20	CXOU J031717.3-410558	3:17:17.30	−41:05:58.4	33.28	5.85±1.38	4.25	3.98
21	CXOU J031720.3-410657	3:17:20.39	−41:06:58.0	35.90	4.88±1.26	3.88	3.32
22	CXOU J031715.5-410609	3:17:15.56	−41:06:09.3	39.23	7.33±1.54	4.76	4.99
23	CXOU J031721.7-410651	3:17:21.70	−41:06:51.9	42.24	32.59±3.25	10.04	22.19
24	CXOU J031718.8-410712	3:17:18.82	−41:07:12.0	43.77	11.93±1.96	6.07	8.12
26	CXOU J031716.9-410709	3:17:16.99	−41:07:09.5	45.02	12.49±2.01	6.21	8.50
27	CXOU J031716.5-410712	3:17:16.52	−41:07:12.7	50.21	15.37±2.23	6.89	10.47
28	CXOU J031717.5-410718	3:17:17.51	−41:07:18.2	51.42	19.85±2.53	7.83	13.52
29	CXOU J031717.5-410724	3:17:17.53	−41:07:24.9	57.81	6.40±1.44	4.45	4.36
30	CXOU J031713.4-410629	3:17:13.46	−41:06:29.6	58.04	9.92±1.79	5.54	6.75
31	CXOU J031723.4-410648	3:17:23.48	−41:06:48.6	58.73	21.63±2.64	8.18	14.73
32	CXOU J031723.2-410709	3:17:23.25	−41:07:09.4	66.75	4.24±1.17	3.62	2.89
33	CXOU J031724.5-410611	3:17:24.57	−41:06:11.2	69.67	6.63±1.46	4.53	4.52
34	CXOU J031721.4-410733	3:17:21.43	−41:07:33.9	73.03	22.39±2.69	8.32	15.24
35	CXOU J031716.6-410512	3:17:16.68	−41:05:12.9	78.46	36.23±3.42	10.58	24.67
36	CXOU J031713.8-410726	3:17:13.82	−41:07:26.1	79.09	34.36±3.33	10.31	23.40
37	CXOU J031725.9-410621	3:17:25.90	−41:06:21.2	82.86	11.33±1.91	5.92	7.72
38	CXOU J031711.5-410714	3:17:11.57	−41:07:14.1	91.65	5.27±1.31	4.04	3.59
39	CXOU J031712.1-410531	3:17:12.10	−41:05:31.3	92.94	6.53±1.45	4.49	4.45
40	CXOU J031719.2-410453	3:17:19.29	−41:04:53.7	94.94	4.83±1.25	3.87	3.29
41	CXOU J031726.3-410544	3:17:26.36	−41:05:44.1	98.22	20.86±2.60	8.03	14.21
42	CXOU J031711.8-410501	3:17:11.89	−41:05:01.1	115.55	3.06±1.00	3.08	2.09
43	CXOU J031722.5-410815	3:17:22.58	−41:08:15.2	115.94	6.67±1.47	4.54	4.54
44	CXOU J031721.7-410434	3:17:21.71	−41:04:34.9	118.76	4.71±1.23	3.82	3.21
45	CXOU J031713.5-410442	3:17:13.54	−41:04:42.5	120.22	4.13±1.16	3.57	2.81
46	CXOU J031724.2-410811	3:17:24.21	−41:08:11.7	121.31	8.43±1.65	5.11	5.74
47	CXOU J031719.0-410423	3:17:19.01	−41:04:23.2	125.15	10.41±1.83	5.67	7.09
48	CXOU J031714.4-410430	3:17:14.45	−41:04:30.2	127.12	3.73±1.10	3.40	2.54

the point sources. Adaptively-smoothed images of the inner $4\farcm5 \times 4\farcm5$ for two energy bands (0.3–1.0 keV and 1.5–6.0 keV) are shown in Figure 2. The images illustrate the major X-ray-emitting components of the galaxy: a very bright central point source (most likely an active galactic nucleus), many fainter point sources (most of which are LMXBs in NGC 1291), and centrally-concentrated diffuse emission that is much more pronounced in the soft band. The diffuse emission is more or less circularly symmetric, although there are some asymmetries at intermediate radii. These asymmetries argue that the origin of most of the soft emission is hot gas rather than from a stellar component (which should be distributed like the optical light). It is unlikely that the majority of the asymmetric diffuse emission is from unresolved sources below the detection limit, since similar diffuse features are not seen in the 1.5–6.0 keV image. Nor is it likely that sources below the detection threshold of this observation have extremely soft spectra, since our preliminary work on sources in the bulge of M31 shows that there is no softening of LMXB spectra for sources with luminosities down to 10^{36} ergs s^{-1}. The gas is contained almost entirely within the optical confines of the bulge, which is shown in Figure 2.

3.2. *Point Sources*

We used the CIAO program WAVDETECT to detect X-ray point sources in OB1 over the 0.3-6.0 keV energy range. A minimum detection threshold of 3σ was adopted. This corresponded to a limiting 0.3–6.0 keV count flux of 3.0×10^{-4} counts s^{-1} and a limiting 0.3–10 keV luminosity of 2.0×10^{37} ergs s^{-1} at the assumed distance of 8.9 Mpc, assuming the spectra of all sources but the central

source are described by a power law with $\Gamma = 1.56$ (see § 4.1 below). Here, we concentrate on the sources seen in projection within the bulge of NGC 1291. A total of 48 sources were detected from the bulge region in OB1, and are listed in Table 1 in order of increasing distance from the center of NGC 1291. For the count–to–luminosity conversion, we assume 1 count $s^{-1} = 6.80 \times 10^{40}$ ergs s^{-1} (0.3–10 keV band) except for the central source, where we assume a spectrum based on the spectral fit for that source (§ 4.3).

We constructed the luminosity function of the bulge X-ray sources. Since the luminosity of LMXBs in our own Galaxy can vary on timescales shorter than a few months, it is unclear whether merging the two observations will lead to an accurate assessment of the luminosity function of the sources in NGC 1291. Ideally one wants the instantaneous distribution of the luminosities, so we analyze only sources detected in the longer of the two observations, OB1 (although it should be noted that the luminosity function of OB1+OB2 was not substantially different from that of OB1 alone). The cumulative luminosity function for the 47 non-central sources detected in OB1 is shown in Figure 3. The central source was not included, as it is most likely an AGN. The luminosity function is roughly a power-law between 3×10^{37} ergs s^{-1} and 2×10^{38} ergs s^{-1}. There is a steep drop off above $\sim 2.5 \times 10^{38}$ ergs s^{-1}. The luminosity function also may flatten somewhat below $\sim 3 \times 10^{37}$ ergs s^{-1}. However, it is possible that this is due to incompleteness near the detection threshold (2.0×10^{37} ergs s^{-1}), which might be due to the increase in the width of the instrumental point-spread function with distance from the center, or to reduced point-source sensitivity in regions of high diffuse surface brightness. Simulations suggest that incompleteness affects the luminosity function up to a luminosity of about 1.5 times the detection threshold (e.g., Blanton, Sarazin, & Irwin 2001). Thus, we will only fit the observed luminosity function for $L_X \geq 3 \times 10^{37}$ ergs s^{-1}.

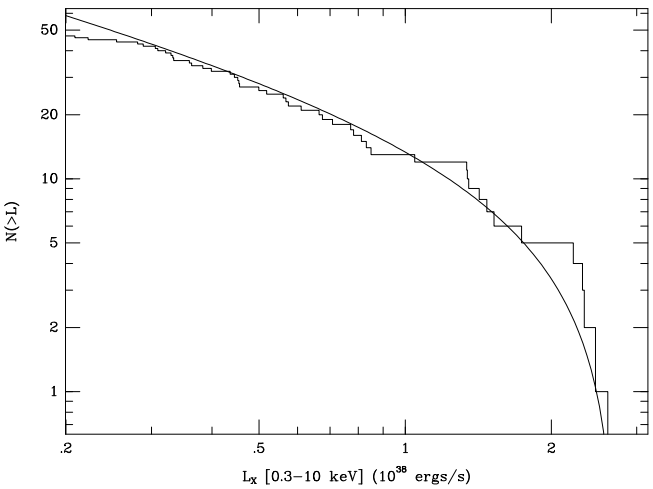

FIG. 3.— Histogram of the cumulative 0.3–10 keV X-ray luminosity function for the 47 point sources within the bulge of NGC 1291 detected in OB1. The central source has been omitted. Roughly three of these sources are expected to be unrelated foreground/background sources. Incompleteness may affect the sources below $\sim 3 \times 10^{37}$ ergs s^{-1}. The solid line is the best-fit cut-off power-law function for the galactic sources (eq. 1).

We used maximum likelihood techniques to fit the luminosity function, as described in SIB00 and Sarazin, Irwin, & Bregman (2001, hereafter SIB01). We modeled unrelated background sources based on *Chandra* deep fields (e.g., Mushotzky et al. 2000); about three such sources are expected in angular area subtended by the bulge. We first tried a single power-law (plus the background sources) model, but it could be rejected at >99% confidence level. The problem with a single power-law is the steep drop above $\sim 2.5 \times 10^{38}$ ergs s^{-1}. Elliptical and S0 galaxies have luminosity functions that are broken power-laws, with the break occurring at about this same luminosity (SIB00; Blanton et al. 2001). Thus, we tried such a broken power-law, and it gave an acceptable fit. However, the power-law exponent above the break was very steep; best-fit exponent was −59. Thus, the NGC 1291 source luminosity function effectively is cut-off above $\sim 2.5 \times 10^{38}$ ergs s^{-1}. We tried fitting the luminosity function as a single power-law with a high luminosity cut-off,

$$\frac{dN}{dL_{38}} = \begin{cases} N_o \left(\frac{L_{38}}{L_c}\right)^{-\alpha} & L_{38} \leq L_c \\ 0 & L_{38} > L_c \end{cases} , \qquad (1)$$

where L_{38} is the X-ray luminosity (0.3–10 keV) in units of 10^{38} ergs s^{-1}, and L_c is the cut-off luminosity. The best-fit values are $L_c = 2.6^{+0.2}_{-0.5} \times 10^{38}$ ergs s^{-1}, $\alpha = 1.56^{+0.32}_{-0.53}$, and $N_o = 3.7^{+4.4}_{-0.9}$. This best-fit cut-off power-law is shown in Figure 3.

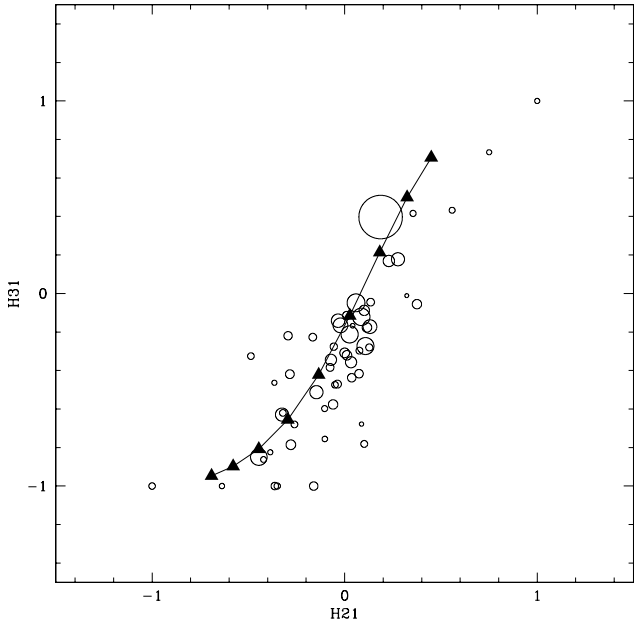

FIG. 4.— X-ray hardness ratios of point sources in NGC 1291, defined as H21=(M–S)/(M+S) and H31=(H–S)/(H+S), where S, M, and H are the counts in the 0.3–1.0 keV, 1.0–2.0 keV, 2.0–6.0 keV energy band, respectively. The area of the circle is proportional to the total flux of the source. The filled triangles represent the colors predicted from a power law model with an exponent $\Gamma = 0$ (upper right) to $\Gamma = 3.2$ in increments of 0.4.

In Figure 4 we plot the X-ray colors of the point sources found in the OB1+OB2 observation for the 48 sources found within the bulge. We define three X-ray bands, S (0.3–1.0 keV), M (1.0–2.0 keV), and H (2.0–6.0 keV), and create two X-ray colors, H21 = (M–S)/(M+S) and H32 = (H–S)/(H+S). These are the same bands and colors defined in SIB00, except for the upper energy limit of

band H, where we exclude energies above 6.0 keV to reduce noise. This has only a minimal effect on H31. The sources occupy a rather narrow band in color space, as was found for the sources in NGC 4697 and NGC 1553 (SIB01; Blanton et al. 2001). The source located at $(-1, -1)$ is a supersoft source, similar to those found in the Large Magellanic Cloud and M31 (e.g., Kahabka & van den Heuvel 1997), and has no detectable emission above 1 keV. The colors predicted from a power law with a range of exponents is also shown in Figure 4. The colors of the central source (largest circle) indicates a rather hard spectrum, although somewhat more band S emission than might be expected. A detailed spectrum of this source is presented in § 4.3 below. Four sources have H31 values of –1 (no band H emission) and H21 between –0.2 and –0.4. Three of these sources are on the outskirts of the bulge and might therefore be unrelated to NGC 1291 (a similar population of sources was found at larger radii in NGC 4697; SIB01).

We compared the positions of the X-ray point sources to objects found on the Digital Sky Survey (DSS) images. None of the 47 non-central point sources in the bulge of NGC 1291 have optical counterparts that are detectable on the DSS images. However, this is not surprising since faint optical sources would be difficult to detect in the high optical surface brightness bulge. Of the 43 sources outside the bulge, only three had optical counterparts within 3″, whose coordinates were obtained from the USNO-A2.0 optical catalog (Monet et al. 1998). All three optical sources were very red, and might be globular clusters belonging to NGC 1291. A significantly higher percentage of the X-ray sources in the outer regions of NGC 4697 and NGC 1553 are potentially associated with a globular cluster than was found for NGC 1291. However, the studies of NGC 4697 and NGC 1553 benefited from globular cluster lists derived from ground-based or *Hubble Space Telescope* data, so it was possible to identify fainter candidate globular clusters. We were unable to find a globular cluster list for NGC 1291 in the literature, and it is likely that several more of the X-ray sources detected in the outer regions of NGC 1291 also belong to globular clusters.

3.3. *Diffuse Emission*

Since the soft band X-ray emission is roughly circularly symmetric, we extracted a radial surface brightness profile in circularly-concentric annular rings centered on the center of NGC 1291, and excluded all point sources detected at the $> 3\sigma$ level. The soft band emission was detectable out to a radius of 120″, after which the emission flattened to a constant value. We chose an annular region $140'' - 170''$ in extent as our background region, being sure to omit the part of this region that was not covered by both observations. The raw and the background-subtracted surface brightness profiles for the soft band are shown in Figure 5.

XSPEC simulations show that 0.32 keV gas (which describes the spectrum of the soft emission; see § 4.2 below), emits a negligible amount of flux above 1.5 keV. Therefore, we can safely assume that the diffuse hard emission is from unresolved point sources below the detection threshold of the observation. In fact, extrapolating the luminosity function (see § 3.2) of the resolved sources down to 10^{35} ergs s^{-1} predicted a value for the luminosity for the unresolved sources that was within 4% of the

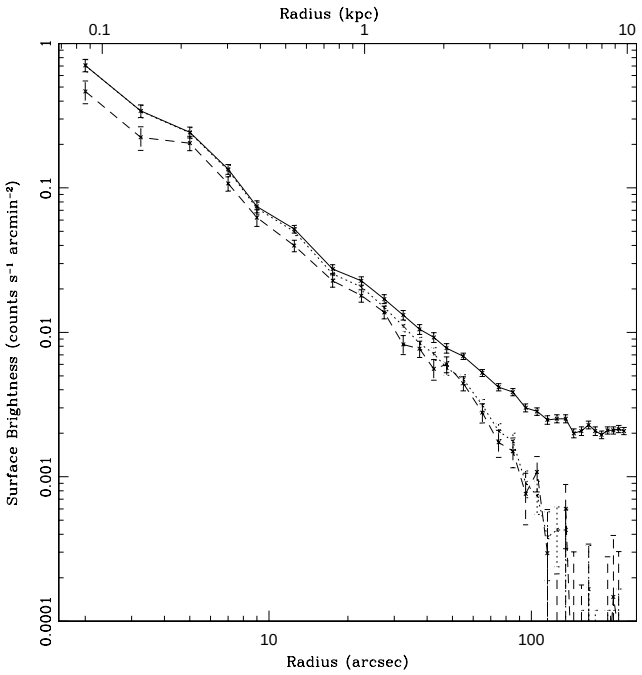

FIG. 5.— Radial surface brightness of the diffuse emission in the 0.3–1.0 keV band, showing the raw profile (*solid line*), background-subtracted profile (*dotted line*), and unresolved source-corrected profile (*dashed line*).

measured value for the diffuse hard emission. The diffuse emission in the soft band, however, is a combination of hot gas and unresolved sources. We can use the observed radial profile of the 1.5–6 keV emission to correct the 0.3–1.0 keV radial profile for stellar contamination. We assume that the ratio of 0.3–1.0 keV/1.5–6.0 keV count flux is the same for the unresolved point sources as it is for the resolved point sources, and multiply the hard radial profile by this ratio

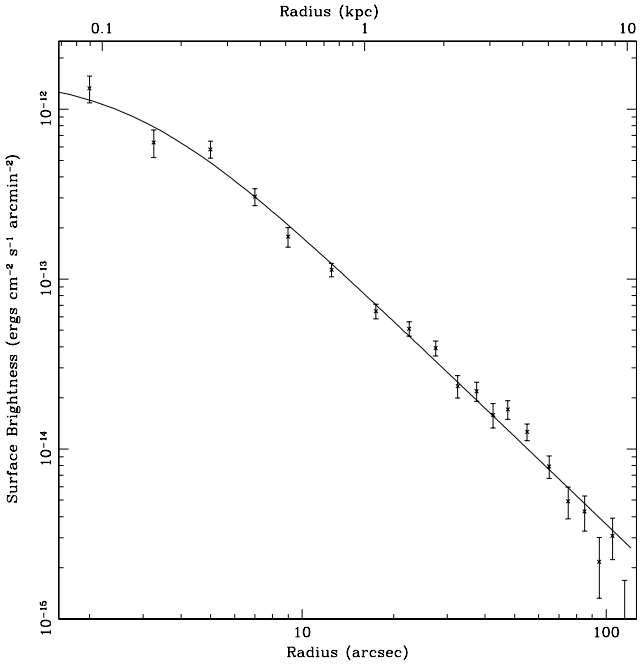

FIG. 6.— Radial surface brightness of gaseous emission in NGC 1291, with best-fit β profile $\beta = 0.45$ and $r_{\rm core} = 2\farcs9$ (125 pc).

before subtracting it from the soft radial profile to

yield the gas-only radial profile. This profile is also shown in Figure 5. We fit a β-profile to the gaseous surface brightness distribution and found best-fit values of $\beta = 0.45^{+0.02}_{-0.01}$ and $r_{\rm core} = 2\farcs9^{+1.1}_{-0.9}$ ($0.125^{+0.043}_{-0.039}$ kpc) (Figure 6). A value of $\beta = 0.45$ is typical for elliptical galaxies (Forman et al. 1985; Trinchieri et al. 1986). Previous studies of elliptical galaxies have found much larger core radii than was found for NGC 1291. However, all these galaxies were quite large, luminous, and rich in hot gas. A recent *ROSAT* HRI analysis of several smaller, X-ray faint galaxies, found core radii similar to the value found here (Brown & Bregman 2001).

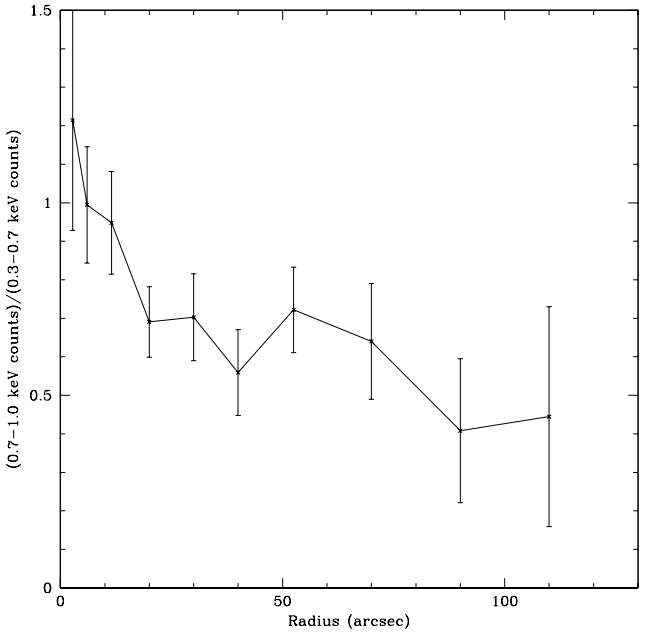

FIG. 7.— Ratio of 0.3–0.7 keV counts to 0.7–1.0 keV counts as a function of radius (1σ uncertainties). The softening of the spectrum with radius indicates a decrease in temperature or a decrease in metallicity, or both.

We extracted the surface brightness profile of the unresolved emission in the 1.5–6 keV band in elliptically-concentric rings that followed the optical light of the galaxy, and found that the diffuse hard X-ray emission was distributed like the optical light (de Vaucouleurs 1975). This is consistent with the idea that the diffuse hard X-ray emission emanates from LMXBs with luminosities below the detection threshold. We also determined the ratio of counts in the 0.7–1.0 keV band to the counts in the 0.3–0.7 keV band (Figure 7). The ratio decreases steeply with radius out to $15''$, and declines more slowly at larger radii. This decline represents either a decline in temperature or a decline in metallicity, and will be investigated further in § 4.2.

4. SPECTRAL ANALYSIS

Previous *Chandra* studies have found that the calibration of the ACIS-S chip is currently suspect below 0.7 keV (Markevitch et al. 2000; SIB01), so we initially fit all spectra only in the 0.7–10 keV energy range. However, it was found that the best-fit 0.7–10 keV spectrum of the point sources provided an adequate fit to the spectrum even when channels down to an energy of 0.5 keV were added. Therefore, we include channels down to 0.5 keV in all subsequent fits. For the diffuse emission, we limited the spectral range to 0.5–6.0 keV to eliminate high background rates at high energies. Background was once again taken from an annular region $140'' - 170''$ in extent. The spectra were regrouped so that each channel contained at least 25 counts. Spectra were extracted from OB1 and OB2 separately and fit within XSPEC 11.0 separately. (Redistribution matrix files (RMF) and ancillary response files (ARF) files were created using the CALCRMF and CALCARF routines of Alexey Vikhlinin for extended sources and with the CIAO task PSEXTRACT for the central point source. All errors given are 90% confidence levels for one interesting parameter ($\Delta\chi^2 = 2.71$). A summary of the spectral fits is given in Table 2.

4.1. *Summed Resolved Point Sources In the Bulge*

In order to avoid excessive contamination from unrelated foreground/background X-ray sources and from disk/spiral arm population X-ray sources of NGC 1291, we analyze only sources projected within the bulge of the galaxy. We also excluded the central source that is most likely an AGN. As noted above (§ 3.2), we would expect only $\sim$3 serendipitous foreground/background sources above our detection threshold within the bulge. A simple bremsstrahlung model with a temperature of $kT = 7.5^{+1.6}_{-1.2}$ keV and the absorption fixed at the Galactic value (1.60×10^{20} cm^{-2}) fit the data adequately ($\chi^2_\nu = 1.17$ for 112 degrees of freedom). A power law model provided a somewhat better fit ($\chi^2_\nu = 1.06$ for 112 degrees of freedom) with $\Gamma = 1.56 \pm 0.05$. A disk blackbody + blackbody model that has been employed to fit the spectra of Galactic LMXBs as well as the summed emission from LMXBs in M31 (Mitsuda et al. 1984) provided an equally acceptable fit ($\chi^2_\nu = 1.06$), but the best fit parameters ($kT_{in} = 0.37$ keV and $kT_{BB} = 1.1$ keV) were unlike those of Galactic LMXBs. Freeing the absorption did not improve the fit. The power law exponent and the bremsstrahlung temperature are in agreement with previous *Chandra* observations of LMXBs in early-type systems (SIB01; Blanton et al. 2001). No excess soft emission was detected in the spectra of the LMXBs. The summed source fluxes from OB1 and OB2 were consistent within the uncertainties, indicating that the effect of variability of the summed source spectrum is small.

4.2. *Diffuse Emission*

The color analysis of the diffuse emission within the bulge indicated the presence of both stellar and gaseous components in the diffuse emission, so we used a two component model consisting of a MEKAL component (Mewe, Gronenschild, & van den Oord 1985; Kaastra & Mewe 1993; Liedahl et al. 1995) to represent the gaseous emission and a power law or thermal bremsstrahlung to represent the unresolved stellar sources. The hard component parameter (Γ or kT) was fixed at the value found for the sum of the resolved sources. The temperature and metallicity of the MEKAL component were allowed to vary. A good fit ($\chi^2_\nu = 1.08$ for 170 degrees of freedom) was obtained with a temperature of $0.32^{+0.04}_{-0.03}$ keV and metallicity of 0.06 ± 0.02 solar when the hard component was a power law model. Nearly identical values were found when a bremsstrahlung or disk blackbody + blackbody

model represented the hard component. The temperature and abundance values were practically independent of the shape of the hard component. Fixing the exponent of the power law at $\Gamma = 1$ or $\Gamma = 2$ led to less than a 5% change in the best-fit temperature.

Next, we extracted spectra from annular regions $1\farcs5 - 15''$ and $15'' - 100''$ in extent, and fit them with a similar model as above. From the inner bin to the outer bin, the temperature declined very slightly from $0.34^{+0.05}_{-0.03}$ keV to $0.30^{+0.04}_{-0.03}$ keV. Interestingly, there was some evidence for decreasing abundance with radius from 0.13 ± 0.04 to $0.05^{+0.04}_{-0.02}$ of the solar value.

4.3. *Central Point Source*

The spectrum from the bright central point source could not be fit well with any single component model in the 0.5–10 keV energy range. However, the emission within the $1\farcs5$ extraction radius is likely contaminated by ∼0.34 keV gaseous emission. Therefore, we fit the spectrum of the central source only over the 1.5–10 keV range where the gaseous emission is negligible. Now the spectrum is fit equally well by a heavily absorbed power law ($\Gamma = 1.93^{+0.37}_{-0.28}$ and $N_H = 2.03^{+0.74}_{-0.69} \times 10^{22}$ cm^{-2}) or thermal bremsstrahlung ($kT = 8.3^{+8.3}_{-3.4}$ keV and $N_H = 1.59^{+0.50}_{-0.48} \times 10^{22}$ cm^{-2}). The power law exponent/bremsstrahlung temperature and the absorption were linked for OB1 and OB2, and allowing them to vary separately did not significantly improve the fit. These values are quite unlike those of the summed non-central point source spectrum in NGC 1291, which was fit well by a thermal model of similar temperature but with only Galactic absorption. The 2–10 keV luminosity of the central source decreased by a factor of two between OB1 and OB2, from 2.9×10^{39} ergs s^{-1} to 1.4×10^{39} ergs s^{-1} (for the power law model). The high variability, a power law index of 1.7–2.0, and heavy (10^{22} cm^{-2}) absorption argues that the source is an obscured low luminosity AGN.

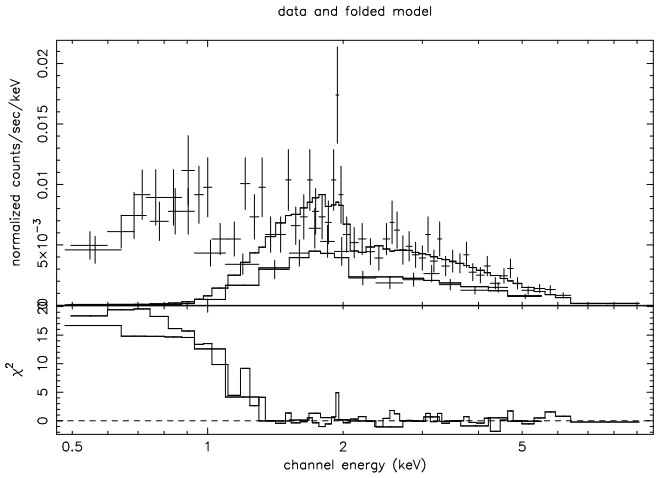

FIG. 8.— Best-fit power law spectrum of the central point source from OB1 and OB2 over the 1.5–10 keV range. Energy channels below 1.5 keV have been added without re-fitting the spectrum to illustrate the excess soft emission. Note that although the power law component differs by a factor of two between OB1 and OB2, the excess soft component flux is the same between the two observations.

After freezing the best-fit parameters, we included channels down to 0.5 keV and noticed excess emission in the 0.5–1.5 keV range (Figure 8). A total of 285 counts were found in excess of the absorbed power law model. Below 1.0 keV the count rates of OB1 and OB2 were the same, indicating a different source of the soft emission than what is producing the variable hard emission. The number of counts below 1.5 keV that is expected within the $1\farcs5$ extraction region from the hot gas (by extrapolating the sur-

TABLE 2
X-RAY SPECTRAL FITS

Component	Model	N_H (10^{20} cm^{-2})	kT or Γ (keV)	Abundance (relative to solar)	χ^2_ν/dof
Sources	bremss	(1.60)	$7.5^{+1.6}_{-1.2}$		1.17/112
Sources	bremss	< 0.64	$8.9^{+2.1}_{-1.6}$		1.11/111
Sources	power	(1.60)	1.56 ± 0.05		1.06/112
Sources	power	< 3.82	1.56 ± 0.09		1.07/111
Gaseous (global)	MEKAL	(1.60)	$0.33^{+0.05}_{-0.03}$	0.04 ± 0.02	1.08/17 0
Gaseous (global)	MEKAL	< 6.02	$0.35^{+0.06}_{-0.05}$	$0.04^{+0.04}_{-0.02}$	1.09/169
Gaseous ($1\farcs5 - 15''$)	MEKAL	(1.60)	$0.35^{+0.05}_{-0.03}$	$0.10^{+0.03}_{-0.02}$	1.65/31
Gaseous ($15'' - 100''$)	MEKAL	(1.60)	$0.30^{+0.04}_{-0.03}$	$0.04^{+0.04}_{-0.02}$	1.14/155
Central source[a]	power	$203.3^{+74.1}_{-69.3}$	$1.93^{+0.37}_{-0.28}$		0.68/48
Central source[a]	bremss	$159.4^{+49.9}_{-48.3}$	$8.3^{+8.3}_{-3.4}$		0.68/48
Central source[b]	MEKAL	(1.60)	$0.75^{+0.12}_{-0.11}$	0.09 ± 0.04	0.76/70
Central source[b]	blackbody	(1.60)	0.21 ± 0.03		0.86/70

[a] 1.5–10 keV only, with normalizations free for OB1 and OB2.

[b] 0.5–10 keV; soft component parameters, after fixing the parameters of the power law component derived in the 1.5–10 keV fit.

face brightness profile of the hot gas to the very center) is only ~ 50 counts. Thus, most of the excess counts must come from a second, soft component of the central source. After fixing the absorption and power law exponent, we added a MEKAL component with a temperature of 0.34 keV to model the hot ISM gas expected in the 1.″5 extraction region, and fixed the normalization so that this component yielded 50 counts. We then added another MEKAL model and allowed the temperature and metallicity to vary. This component was absorbed by a column density equal to the Galactic column density in that direction. The best-fit MEKAL temperature was $kT = 0.75^{+0.12}_{-0.11}$ keV and the best-fit metallicity was 0.09 ± 0.04 solar ($\chi^2_\nu = 0.76$ for 69 degrees of freedom). Substituting a blackbody model for the second MEKAL model yielded a somewhat worse but still acceptable fit with $kT_{BB} = 0.21 \pm 0.03$ keV. The luminosity of the soft component was 1.5×10^{38} ergs s^{-1}, or 5%–10% of the hard component luminosity.

5. DISCUSSION

5.1. *A Comparison of the Stellar L_X/L_B Ratio of NGC 1291, NGC 4697, and NGC 1553*

Previous work has indicated that the stellar X-ray–to–optical luminosity ratio is not the same in all galaxies. In a survey of 61 early-type galaxies observed by *ROSAT*, Irwin & Sarazin (1998b) found that eight galaxies had extremely low L_X/L_B values, over a factor of three less than the L_X/L_B value of the bulge of M31 and other X-ray faint early-type galaxies whose X-ray emission we now know to be composed primarily of of LMXBs with only a small amount of gas such as NGC 4697 (Primini et al. 1993; Shirey et al. 2001; SIB01). If all the gas were removed from NGC 4697, for example, its L_X/L_B ratio would decrease by only a factor of ~ 1.4 in the *ROSAT* band. Since eight galaxies in the Irwin & Sarazin (1998b) sample had L_X/L_B values at least a factor of three below that of M31 or NGC 4697, this implied that the production of LMXBs in early-type systems is different from galaxy to galaxy, and that the X-ray luminosity from stellar sources does not scale linearly with the optical luminosity. The spatial resolution of *ROSAT* was too coarse to test this hypothesis directly, since individual LMXBs could not be resolved. It was not known if the discrepancy in the LMXB population resulted from a lack of LMXBs at all luminosities or just at the high end of the luminosity distribution.

Chandra's superb spatial resolution allows us to distinguish between the two scenarios. The total (resolved plus unresolved) stellar L_X/L_B value for NGC 1291 is estimated to be 5.3×10^{29} ergs s^{-1} $L_\odot^{-1}$ (of which 71% is resolved in our observation). In the 0.5–2.0 keV (*ROSAT*) band, this stellar L_X/L_B value is 1.5×10^{29} ergs s^{-1} $L_\odot^{-1}$. Using the source list as well as the estimated emission from unresolved point sources from the *Chandra* observation of NGC 4697 (SIB01), we found the total stellar L_X/L_B value for NGC 4697 within one effective (half-optical light) aperture was 7.5×10^{29} ergs s^{-1} $L_\odot^{-1}$ (it is easiest to deal only with sources within the effective aperture in large galaxies like NGC 4697, since the number of contaminating serendipitous sources is much smaller within this angular region than from over the entire optical extent of the galaxy). A similar exercise within two effective radii for NGC 1553 (Blanton et al. 2001) yielded a value of 7.2×10^{29} ergs s^{-1} $L_\odot^{-1}$. In all three galaxies, the central source was omitted. From the luminosity distribution function of NGC 1291 (Figure 3) it is apparent that this difference can be attributed to a lack of bright sources in NGC 1291. In fact there are no sources in NGC 1291 brighter than 3×10^{38} ergs s^{-1}. Direct comparison with NGC 4697 and NGC 1553 indicates that the lack of sources above 3×10^{38} erg s^{-1} in NGC 1291 is probably not the result of low number statistics. Within the inner effective apertures of NGC 4697 and NGC 1553, there are 10 sources each with luminosities greater than 3×10^{38} erg s^{-1} (neglecting central sources that might be AGN). Given that the ratio of optical luminosities within the effective aperture of NGC 4697 and NGC 1553 to the optical luminosity of the entire bulge of NGC 1291 is 1.17 and 2.34, respectively, we would expect 3.7–7.3 sources in NGC 1291 above this luminosity. If we include all sources detected in the field, the number of sources above this luminosity grows to 19 and 35 for NGC 4697 and NGC 1553, respectively, again predicting ~ 7 sources in the bulge of NGC 1291. In NGC 4697, NGC 1553, and NGC 1399 (R. Mushotzky & L. Angelini, private communication) there was a break or "knee" in the luminosity distribution function around a luminosity of 3×10^{38} erg s^{-1}. This luminosity is also approximately the Eddington luminosity of a 1.4 $M_\odot$ neutron star. SIB00 suggest that this break represents a division between LMXBs with black hole and neutron star accreters. If this interpretation is correct, it would mean that NGC 1291 does not have any black hole binaries accreting near the Eddington limit. It is worth noting that the inner 5′ of the bulge of the spiral galaxy M31 also does not contain any X-ray source more luminous than 3×10^{38} ergs s^{-1} (Primini et al. 1993; after converting their 0.2–4.0 keV luminosity to 0.3–10 keV luminosity).

Another illustrative way of presenting the luminosity distribution function is shown in Figure 9*a*, where we have plotted the cumulative L_X/L_B value of sources in the galaxy as a function of increasing L_X. Since we have normalized the X-ray luminosity of the sources by the optical luminosity of the galaxy we can now compare the curve to those of other galaxies. Figure 9*a* also shows the same quantity for the inner effective aperture of NGC 4697 and within two effective radii for NGC 1553. Note that the y-intercept of each curve represents the *unresolved* source L_X/L_B value, a quantity set by the limiting luminosity of the observation (i.e., the curves would go to zero if every last faint LMXB could be detected). Since the determination of L_B is crucial in this comparison, we did not attempt to gauge L_B from the bulge assuming a specific bulge-disk decomposition for NGC 1291. Instead we only included X-ray sources within a circular aperture of 131.″0, for which the integrated B magnitude within this aperture was 10.13 (using photometry values listed in the compilation of Prugniel & Heraudeau 1998). The Galactic reddening maps of Schlegel, Finkbeiner, & Davis (1998) indicated an absorption of $A_B = 0.056$ magnitude. Correcting for foreground reddening and assuming a distance of 8.9 Mpc, we determined an optical luminosity of 1.08×10^{10} $L_\odot$. Schlegel et al. (1998) claim a mean uncertainty of 16% of $A_B = 0.056$, or 0.009 magnitude. This amounts to only a 1% uncertainty in L_B that results from uncertainties associated with foreground extinction corrections.

Two striking features stand out in Figure 9*a*. The total

cumulative L_X/L_B value of NGC 1291 is a factor of 1.4 less than NGC 4697 and NGC 1553. As mentioned above, this is the result of a lack of very luminous sources in

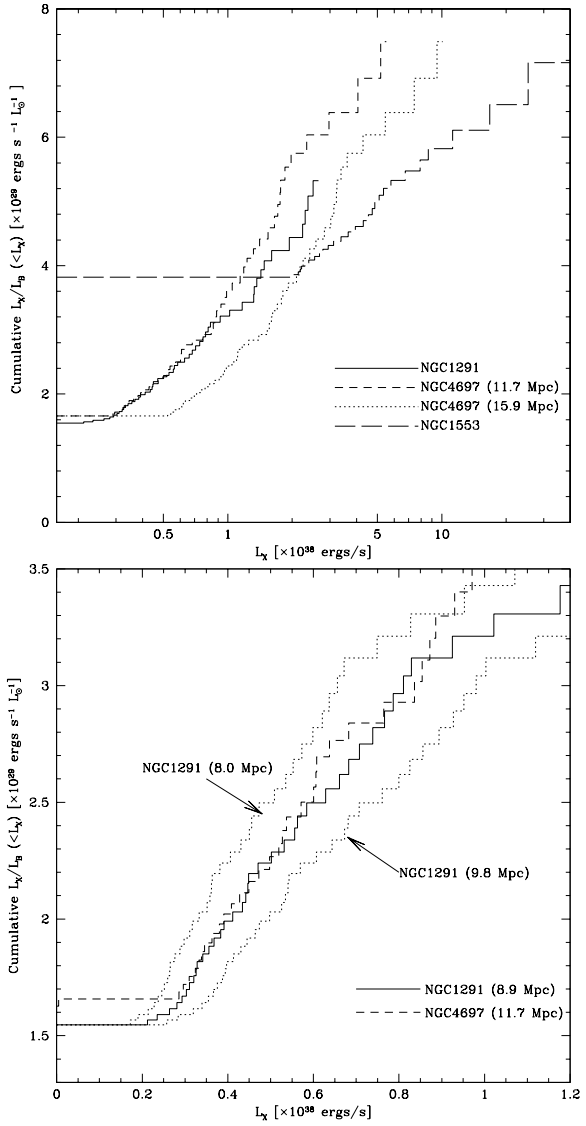

FIG. 9.— (*a*) Cumulative L_X/L_B values as a function of increasing L_X for LMXBs in NGC 1291, NGC 4697 (for distances of 15.9 Mpc and 11.7 Mpc), and NGC 1553. Note the disparity in the number of high luminosity LMXBs among the three galaxies. (*b*) A closer view of the lower left corner of Figure 9*a*, showing the agreement in the cumulative L_X/L_B value of LMXBs in NGC 1291 and NGC 4697 (when a distance of 11.7 Mpc is chosen). Changing the distance of NGC 1291 by $\pm 10\%$ destroys this agreement, and suggests that this agreement might be used as a relative distance indicator.

NGC 1291. This is surprising considering the optical characteristics of early-type systems are very similar. However, for some reason NGC 1291 does not have any of the brightest (probable) black hole binaries that other galaxies have. All three galaxies show a substantial spread in the number and luminosity of sources above 3×10^{38} ergs s^{-1}, the break luminosity discussed above. Also, below 10^{38} ergs s^{-1} the slope of the cumulative L_X/L_B values of NGC 1291 and NGC 4697 are quite similar (NGC 1553 is too distant and the observation time was too short to test this with this galaxy too). In fact, if the distance to NGC 4697 is changed from 15.9 Mpc (the distance assumed by SIB01, which is the recessional velocity distance determined using a value of $H_0 = 50$ km s^{-1} Mpc^{-1}; Faber et al. 1989) to 11.7 Mpc (the distance implied by the surface brightness fluctuation method; Tonry et al. 2001), the agreement in the cumulative L_X/L_B profiles of NGC 1291 and NGC 4697 at low luminosities is remarkable. This indicates that the number of faint LMXBs agrees quite well between the two galaxies, if the smaller distance for NGC 4697 is adopted.

The discrepancy in the number of luminous sources in NGC 1291 can be reconciled with those of NGC 4697 and NGC 1553 if we assume a larger distance to NGC 1291 than 8.9 Mpc. If we increase the distance by 40% to 12.5 Mpc, we find nine sources above 3×10^{38} erg s^{-1}. However, this creates another problem. Although the total cumulative L_X/L_B value is independent of distance, the curve shifts to the right when the distance is increased. When the distance to NGC 1291 is changed from 8.9 Mpc, the agreement in the cumulative L_X/L_B value below 10^{38} ergs s^{-1} is destroyed. Regardless of the chosen distance, the data conclusively show that the production of LMXBs in NGC 1291 differs from that in NGC 4697. If the distance is set to match the low end of the luminosity distribution function, too few bright sources are produced in NGC 1291. If the distance is set to match the high end, too few fainter ($< 10^{38}$ erg s^{-1}) sources are produced in NGC 1291. Moreover, the shape of the upper end of the luminosity function of NGC 1291 disagrees with that of NGC 4697 (§ 3.2), independent of the distance.

Assuming the distances of 8.9 Mpc and 11.7 Mpc to NGC 1291 and NGC 4697, respectively, are correct, the excellent agreement in the cumulative L_X/L_B value below 10^{38} ergs s^{-1} between NGC 1291 and NGC 4697 (Figure 9*a*) suggests that this feature can be used to estimate the distance to nearby galaxies. If the cumulative L_X/L_B value below 10^{38} ergs s^{-1} is a constant from galaxy to galaxy, the point where the cumulative L_X/L_B value begins to diverge might be used as a standard candle. Using X-ray binaries as a standard candle is not a new concept. Margon & Ostriker (1973) suggested that the luminosity of X-ray sources in galaxies could be limited by the Eddington luminosity based on observations of X-ray sources in the Local Group. More recently, SIB00 suggested that the break in the luminosity distribution function at 3×10^{38} ergs s^{-1} might be used as a distance indicator too. The accuracy of this method, however, would always be limited by the relatively small number of sources above the break. The statistics on sources below the break are generally much better, and are further improved by the summing up the luminosities. What is required observationally is to resolve the luminosity function down to $\lesssim 10^{38}$ ergs s^{-1}, and to determine accurately the total amount of X-ray emission from unresolved sources. This method could be used in conjunction with the break in the luminosity function method of SIB00 for greater accuracy. Figure 9*b* zooms in on the lower left corner of Figure 9*a*, illustrating how sensitive the cumulative L_X/L_B–L_X relation is to distance. Changing the assumed distance of NGC 1291 by $\pm 10\%$ leads to an easily measurable difference in the cumulative L_X/L_B values of NGC 1291 and NGC 4697. Of course claims of the validity of this method are premature con-

sidering that only two galaxies have been tested thus far. Many more galaxies will need to be compared to NGC 1291 and NGC 4697 to confirm this method. However, should this method be valid, distances to nearby galaxies can be determined to better than 10% accuracy, and would be one of the very few non-optical methods for determining distances to galaxies. We point out that the cumulative L_X/L_B method is a relative distance estimator, while the method using the break in the luminosity function is an absolute distance estimator. Admittedly, the distance to NGC 1291 is not known with great accuracy, but if this distance estimator method works, we can determine accurate relative distances to these galaxies. In future work, we will study galaxies for which multiple distance estimators already exist and agree with one another and apply our method to them. Also useful will be galaxies that are known to be at the same distance (owing to their group membership).

Recently, White, Kulkarni, & Sarazin (2002; in preparation) have found a correlation between the total LMXB L_X/L_B value and the specific frequency of globular clusters in a galaxy. In addition, Angelini, Loewenstein, & Mushotzky (2001) found that 70% of the X-ray point sources found in a portion of NGC 1399 for which *Hubble* data existed were coincident with globular clusters of NGC 1399. Both these results would seem to be at odds with the idea that the cumulative L_X/L_B profile below 10^{38} ergs s^{-1} is uniform from galaxy to galaxy. One might expect L_X to scale with the globular cluster specific frequency in addition to the optical luminosity L_B rather than L_B alone, rendering the distance estimator method useless in its current form. However, it is possible that both theories are correct. It is known that the specific frequency of globular clusters decreases with decreasing radius in galaxies (Forbes et al. 1996), indicating that the spatial distribution of the globular clusters is more extended than the optical light. For example, the specific frequency of globular clusters in NGC 3115 decreases from 3.1 ± 0.5 to 1.3 ± 0.1 in moving from the outer to the inner regions of the galaxy (Kundu & Whitmore 1998). Therefore, globular cluster X-ray sources might be relatively rare in the inner regions of elliptical galaxies (or bulges), while comprising a larger percentage of the X-ray source population at larger radii (20% in the case of NGC 4697; SIB01). If this is the case, galaxies with high globular cluster specific frequencies would have higher L_X/L_B values than galaxies with low globular cluster specific frequencies because of a higher number of globular cluster X-ray sources at large radii. At smaller radii (such as within the bulge or one effective radius of a galaxy) where non-globular cluster X-ray sources dominate, the L_X/L_B value might be a constant from galaxy to galaxy, allowing the distance indicator method to be utilized. A search for globular clusters in the inner regions of elliptical galaxies with *Hubble Space telescope* would be useful in definitively determining the significance of globular cluster X-ray sources to the total LMXB population and resolving this issue.

5.2. *The Hot Gas within NGC 1291*

The ability to separate the stellar emission from gaseous emission has only become possible since the launch of *Chandra*. Whereas in X-ray bright galaxies the contribution from LMXBs is minimal, such a separation becomes important as the gaseous component becomes less dominant. For example, the *ROSAT* PSPC spectrum of NGC 1291 could be fit equally well with a two-component Raymond-Smith + bremsstrahlung model with $kT_{\rm RS} = 0.15$ keV, $Z = Z_\odot$ and $kT_{\rm brem} = 1.07$ (Bregman et al. 1995) as it could with just a Raymond-Smith model with $kT_{RS} = 0.55$ keV and $Z = 0.01$ solar (Read, Ponman, & Strickland 1997). In both cases, the inability of *ROSAT* to resolve out the binaries and especially the luminous, highly absorbed AGN led to an erroneous measurement of the temperature of the diffuse hot gas. Inaccuracies in the temperature and flux of the hot gas subsequently adversely affects the determination of quantities such as the $L_{X,gas} - L_B$ relation and the $kT_{gas} - \sigma$ relation, both of which have been used to characterize the history and evolution of the hot gas within early-type systems.

Given the spectral and spatial results above, we conclude that 33% (41%) of the counts and 14% (27%) of the 0.3–10 keV (0.3–2 keV) luminosity emanates from a truly diffuse, gaseous component. The 0.3–10 keV X-ray luminosity of the gas is 1.4×10^{39} ergs s^{-1}, leading to a gaseous L_X/L_B value of 1.3×10^{29} ergs s^{-1} $L_\odot^{-1}$. Such a value is quite low compared to X-ray bright elliptical galaxies, but similar to the values found for X-ray faint ellipticals and the bulge of M31 (SIB01; Shirey et al. 2001). Given the velocity dispersion of the bulge of NGC 1291 of 162 km s^{-1} (Dalle Ore et al. 1991), the derived temperature of the gas of 0.32 keV falls very close to the best-fit $kT_{gas} - \sigma$ relation of Davis & White (1996), but considerably above the best-fit relation of Brown & Bregman (1998). The measured temperature is well above the temperature predicted from the velocity dispersion of 0.17 keV, if the thermal energy of the gas were equal to the kinetic energy of the random motions of the stars.

The beta-model for the surface brightness profile of the gas can be inverted to obtain the density profile, $n(r) = n_0[1 + (r/r_{\rm core})^2]^{-3\beta/2}$. Using the best-fit values of the gaseous surface brightness profile of $\beta = 0.45$ and $r_{\rm core} = 2\farcs9$, we derive a central electron density of $n_0 = 0.28$ cm^{-3}. This value is quite high when compared to values obtained for early-type systems with previous instruments (e.g., Rangarajan et al. 1995). However, the $0\farcs5$ spatial resolution of *Chandra* coupled with the nearness of NGC 1291 allows us to probe the electron density profile on the scale of $\sim$50 pc (note that at the distance of the Virgo cluster the core radius would be only $1\farcs3$, far below the resolution limit of previous X-ray telescopes). The implied mass of the gas (assuming a volume filling factor of one) within a radius of $120''$ is 5.8×10^7 M$_\odot$. This value is substantially smaller than the derived gas masses of big bright elliptical galaxies, which tend to be as high as 10^{11} M$_\odot$. The cooling time of the gas at the center of the galaxy is 1.2×10^7 years, and remains less than a Hubble time out to the extent to which the gaseous emission can be detected ($120''$).

Given the relative isolation of NGC 1291, it would appear that the lack of a substantial amount of X-ray emitting gas in the bulge is not the result of recent interaction with a cluster or another galaxy. This result is in accordance with the findings of Brown & Bregman (2000) that optically less luminous galaxies in lower density environments are X-ray faint. In smaller galaxies (or bulges) in non-cluster environments, supernovae-driven winds can

clear the system of much of the gas that might have been pressure-contained by intracluster gas had the galaxy resided in a cluster environment.

Finally, the metallicity of the hot gas in early-type systems has been a longstanding controversy. Optical measurements of the metallicity of stars indicate abundances of solar or greater in elliptical galaxies and the bulges of spiral galaxies. Yet, many measurements of the metallicity of the X-ray gas, particularly those determined with *ASCA*, have yielded values of the metallicity of $\lesssim 20\%$ for many galaxies. Several explanations have been set forth to account for this discrepancy. Buote (1999) suggests that the low measured metallicity of the X-ray gas with *ASCA* is an artifact of fitting the spectra with isothermal models. Multi-temperature models, either due to local multiphase gas or a temperature gradient, would result in higher abundances, at least in the case of the brightest X-ray elliptical galaxies. Finoguenov & Jones (2000) also point out that the angular scales of the optical and X-ray metallicity are different; whereas integrated optical metallicities are typically measured within an arcminute or less for galaxies at the distance of Virgo, X-ray measurements are typically average over $\sim 3'$ bins. Given that the optically-determined metallicities often decline significantly with radius (Carollo, Danziger, & Buson 1993), the stellar metallicity might actually be subsolar at large distances for the center of the galaxy. Furthermore, the *Chandra*-determined abundance profile of the elliptical galaxy NGC 4374 peaked toward the center to a value of 0.6 solar within a 0.5–5 kpc annulus, and declined at larger radii (Finoguenov & Jones 2001). Both the multi-component temperature argument and the mismatch of angular size argument seem to resolve the discrepancy between the metallicity measurements in the much-studied X-ray bright early-type galaxies. However, neither explain the low metallicity found here for NGC 1291. The metallicity from the $1\farcs5 - 15''$ annulus is only 0.13 ± 0.04 solar. An optical measurement of the metallicity of the bulge found it to have an Mg_2 index of 0.24 magnitudes (Golev & Prugniel 1998) corresponding to Fe/H = 1.1 solar (Terlevich et al. 1981). In addition, there appears to be no temperature gradient or evidence for cooling gas in the center of NGC 1291 to bias the metallicity determination of the gas. It appears that X-ray faint systems like NGC 1291 (and NGC 4697, although only a global metallicity was determined; SIB01) really do have low metallicity gas even at their centers.

5.3. *The Central Source*

The presence of a bright, central X-ray point source is somewhat surprising considering there is little evidence in the literature that NGC 1291 hosts an AGN. While not as luminous as other low luminosity AGN, the spectral parameters of the central X-ray source are very similar to those found for a sample of low luminosity AGNs, LINERS, and starbursts observed by *ROSAT* and *ASCA* by Ptak et al. (1999). Such spectral parameters are also common among narrow-line Seyfert 1 galaxies (Reeves & Turner 2000). It should be noted that in these systems the X-ray luminosity of the AGN is at least a factor of ten higher than the AGN in NGC 1291. What is even more surprising is that the flux of the soft component was unchanged between OB1 and OB2, while the hard component decreased in intensity by a factor of two over the same time period. The excellent spatial resolution of *Chandra* confirms that the origin of the soft component lies within ~ 60 pc from the central source, and is almost assuredly associated with the central source.

This kind of temporal behavior in the soft and hard components has also been seen in the narrow-line Seyfert 1 galaxy Mrk 766 with *XMM-Newton* by Page et al. (2001). These authors find that the soft X-ray excess, as well as the ultraviolet emission observed with *XMM-Newton's* Optical Monitor varied very little throughout the observation, whereas the hard continuum component varied significantly. It is unlikely that the soft component can be reprocessed hard power law emission, since in this case the fluxes of the hard and soft components should vary together. It is possible that the soft emission emanates directly from the hot inner accretion disk (Malkan & Sargent 1982) and is the high energy tail of the ultraviolet bump seen in these objects. Alternatively, the source of the soft X-ray emission may be the Compton up-scattering of the ultraviolet photons from this disk.

The detection of a low luminosity active nucleus in NGC 1291 also explains the detection of unresolved 60 micron and 100 micron emission in this galaxy (Rice et al. 1988). Bregman et al. (1995) point out that it was surprising that very little if any CO emission was detected in this galaxy given the 100 micron flux of 10.7 Jy, based on the observed correlation of CO with 100 micron emission in other galaxies. It is quite possible that the 100 micron emission is associated with the AGN and not with dust associated with star formation in the bulge.

5.4. *Hot vs. Cold Gas in Sa Galaxies*

The ratio of hot to cold gas is a strong function of galaxy morphological type. The interstellar material in late-type spiral galaxies is predominantly atomic and molecular with trace amounts of hot gas, while in elliptical galaxies it is just the opposite, with S0 galaxies having a roughly equal mixture of the two (e.g., Bregman, Hogg, & Roberts 1992). As an Sa galaxy, we would expect NGC 1291 to have more cold gas than hot gas. This is indeed the case here, where the mass of the hot gas is 5.8×10^7 $M_\odot$, while the H I gas mass is 1.3×10^9 $M_\odot$ (van Driel, Rots, & van Woerden 1988).

The H I distribution in NGC 1291, as is the case with several S0 and Sa galaxies, is ring-like in nature (van Driel et al. 1988). The central hole in the H I is 7 kpc in radius. An analysis of *ROSAT* PSPC data by Bregman et al. (1995) found that the X-ray emission appears to fill this hole. We confirm this result with our *Chandra* observations; hot, diffuse gas with a temperature of $\sim$0.3 keV is detected out to a radius of 5 kpc.

Whether the hot gas has actually displaced the cold gas or whether it is merely the case that cold gas is a disk phenomenon while hot gas is a bulge phenomenon is still an open question. As Bregman et al. (1995) point out, if the hot and cold gas are thermally coupled, convection and turbulent mixing can lead to the conversion of hot gas to cold gas and vice versa, causing the the two phases to be spatially anticorrelated, with the phase with the higher column density winning out. A signature of this would be a softening of the spectrum of the hot gas with increasing

radius, as successively more hot gas is cooled by the presence of cold gas. Indeed, there is a softening of the 0.7–1.0 keV/0.3–0.7 keV ratio with increasing radius (Figure 7), although it should be noted that the softening occurs at a radius in which there is no detectable H I emission. A more definitive answer might be obtained with an Sa or S0 galaxy that does not have such a large hole in its H I distribution. Several galaxies in the H I sample of van Driel & van Woerden (1991) show complex H I morphology in the center of the galaxy. A high resolution *Chandra* observation of the bulges of these galaxies might shed some light on the interaction (or lack of interaction) between the hot and cold phases of the interstellar medium. If the two phases were thermally isolated, the cold gas would absorb soft X-rays from the hot gas behind it, leading to a hardening of the X-rays in the direction of the H I knots. Alternatively, if the phases are thermally coupled, we might expect the the X-ray gas to fill the empty pockets in the H I distribution, indicating that cold gas has been turned into the hot phase in these regions.

6. CONCLUSIONS

Analyses of two *Chandra* observations of the bulge-dominated spiral NGC 1291 have revealed the primary X-ray–emitting components of the galaxy. The bulk of the X-rays (by counts and by luminosity) emanates from a collection for several dozen LMXBs that exhibit a range of spectral characteristics. A significantly smaller fraction of the X-ray emission comes from a 0.32 keV thermal gas with low metallicity. These observations demonstrate, along with *XMM-Newton* observations of the bulge of M31 (Shirey et al. 2001), that the X-ray emission of bulges of galaxies resemble that of a sub-class of elliptical and S0 galaxies that are X-ray faint. The rather high temperatures measured for Sa galaxies with *Einstein* (Kim et al. 1992) were the result of the mixture of two spectrally distinct components, namely LMXBs and hot gas.

The luminosity distribution function of LMXBs in the bulge of NGC 1291 can be compared to that of other early-type galaxies to explore differences in the LMXB populations from galaxy to galaxy. There are no LMXBs with luminosities greater than 3×10^{38} ergs s^{-1} in NGC 1291, where about seven were expected by scaling from NGC 4697 or NGC 1553. This lack of high luminosity LMXBs is the cause of the wide spread in the stellar L_X/L_B values seen with previous X-ray instruments. Such a spread suggests that the production of LMXBs with massive primaries is not uniform from galaxy to galaxy, despite the uniformness of the present-day stellar population among early-type systems. On the other hand, below 10^{38} ergs s^{-1} there is remarkable agreement in the LMXB functions of NGC 1291 and NGC 4697. This agreement is highly sensitive to the assumed distance of NGC 1291. If this agreement is a generic property of LMXBs in early-type systems, it can be used as an accurate distance indicator, one of the very few non-optical methods for determining galactic distances.

The distribution of the hot gas can be described by the standard β profile with $r_{\rm core} = 2\farcs9$ and $\beta = 0.45$. The central density of the gas is 0.28 cm^{-3}, and the total mass of the gas is 5.8×10^7 M$_\odot$, far less than the mass of the H I in the galaxy. There is marginal evidence that the temperature and metallicity decrease slightly outside of 0.6 kpc. The temperature of the gas, while lower than in X-ray bright galaxies, is similar to that in other X-ray faint systems such as NGC 4697 and the bulge of M31 (SIB01; Shirey et al. 2001). The paucity of gas in the system is probably the result of the removal of most of the gas by supernovae-driven winds rather than interaction with a cluster environment. The low measured metallicity of the gas is in conflict with the optically-determined value of the metallicity of the bulge. The hot gas fills the hole in the H I distribution, possibly indicating that the hot gas has displaced the cold gas in the overlap region. However, future observations of Sa galaxies with smaller H I holes will be able to address this issue more conclusively.

Finally, the central point source is coincident with the optical center of the galaxy, and exhibits significantly different spectral characteristics than the sum of the other resolved point sources. Above 1.5 keV, the spectrum is adequately described by a highly absorbed ($N_H > 10^{22}$ cm^{-2}) power law with $\Gamma = 1.9$, and the luminosity varied by a factor of two between the two observations. Below 1.5 keV, there is an excess of soft photons over what is expected from hot gas within the extraction region. The soft component is of equal strength in the two observations, and can be modeled by a MEKAL model with a temperature of 0.75 keV and low metallicity, and has a luminosity that is 5%–10% that of the hard component. The parameters of both the hard and soft components are very similar to those of low luminosity AGNs studied previously with *ASCA* and *ROSAT* (Ptak et al. 1999).

We thank the referee, Rene Walterbos, for many insightful comments and suggestions that improved the manuscript considerably. We thank Jonathan McDowell for his help in implementing the CALCRMF and CALCARF routines of Alexey Vikhlinin for spectral analysis. We thank David Buote and Elizabeth Blanton for useful conversations and suggestions. J. A. I. was supported by *Chandra* Fellowship grant PF9-10009, awarded through the *Chandra* Science Center. C. L. S. was supported in part by *Chandra* Award Numbers GO0-1141X, GO0-1158X, GO0-1173X, and GO1-2078X, all issued by the *Chandra* Science Center. J. N. B. was supported by *Chandra* Award Number GO0-1148X. The *Chandra* Science Center is operated by the Smithsonian Astrophysical Observatory for NASA under contract NAS8-39073.

REFERENCES

Angelini, L., Loewenstein, M., & Mushotzky, R. F. 2001, ApJ, 557, L35
Blanton, E. L., Sarazin, C. L., & Irwin, J. A. 2001, ApJ, 552, 106
Bregman, J. N., Hogg, D. E. , & Roberts, M. S. 1992, ApJ, 387, 484
Bregman, J. N., Hogg, D. E. , & Roberts, M. S. 1995, ApJ, 441, 561
Brown, B. A., & Bregman J. N. 1998, ApJ, 495, L75
Brown, B. A., & Bregman J. N. 2000, ApJ, 539, 592
Brown, B. A., & Bregman J. N. 2001, ApJ, 547, 154
Buote, D. A. 1999, MNRAS, 309, 685
Carollo, C. M., Danziger, I. J., & Buson, L. 1993, MNRAS, 265, 553
Dalle Ore, C., Faber, S. M., Jesus, J., Stoughton, R., & Burstein, D. 1991, ApJ, 366, 38
Davis, D. S., & White, R. E. III 1996, ApJ, 470, L35
de Vaucouleurs, G. 1975, ApJS, 29, 193

Faber, S. M., Wegner, G., Burstein, D., Davies, R. L., Dressler, A., Lynden-Bell, D., & Terlevich, R. J. 1989, ApJS, 69, 763
Finoguenov, A., & Jones, C. 2000, ApJ, 539, 603
Finoguenov, A., & Jones, C. 2001, ApJ, 547, L107
Forbes, D. A., Franx, M., Illingworth, G. D., & Carollo, C. M. 1996, ApJ, 467, 126
Forman, W., Jones, C., & Tucker, W. 1985, ApJ, 293, 102
Golev, V., & Prugniel, Ph. 1998, A&AS, 132, 255
Hogg, D. E., Roberts, M. S., Bregman, J. N., & Haynes, M. P. 2001, AJ, 121, 1336
Irwin, J. A., & Sarazin, C. L. 1998a, ApJ, 494, L33
Irwin, J. A., & Sarazin, C. L. 1998b, ApJ, 499, 650
Kaastra J. S., & Mewe R. 1993, A&AS, 97, 443
Kahabka, P., & van den Heuvel, E. P. J. 1997, ARA&A, 35, 69
Kambas, A., Davies, J. I., Smith, R. M., Bianchi, S., & Haynes, J. A. 2000, AJ, 120, 1316
Kim, D. -W., Fabbiano, G. , & Trinchieri, G. 1992, ApJ, 393, 134
Kundu, A., & Whitmore, B. C. 1998, AJ, 116, 2841
Liedahl D. A., Osterheld A. L., & Goldstein W. H. 1995, ApJ, 438, L115
Malkan, M. A., & Sargent, W. L. W. 1982, ApJ, 254, 22
Margon, B., & Ostriker, J. P. 1973, ApJ, 186, 91
Markevitch et al. 2000, ApJ, 541, 542
Matsumoto, H., Koyama, K., Awaki, H., & Tsuru, T., Loewenstein, M., & Matsushita, K. 1997, ApJ, 482, 133
Mewe R., Gronenschild E. H. B. M., & van den Oord G. H. J. 1985, A&AS, 62, 197
Mitsuda, K., Inoue, H., Koyama, K., Makishima, K., Matsuoka, M., Ogawara, Y., Suzuki, K., Tanaka, Y., Shibazaki, N., & Hirano, T. 1984, PASJ, 41, 97
Monet D., et al., 1998, USNO-A V2.0, A Catalog of Astrometric Standards (Flagstaff: U.S. Naval Observatory)
Mushotzky, R. F., Cowie, L. L., Barger, A. J., & Arnaud, K. A. 2000, Nature, 404, 459
Page, M. J., et al. 2001, A&A, 365, L152
Primini, F. A., Forman, W., & Jones, C. 1993, ApJ, 410, 615
Prugniel, P., & Heraudeau, P. 1998, A&AS, 128, 299
Ptak, A., Serlemitsos, P., Yaqoob, T., & Mushotzky, R. 1999, ApJS, 120, 179
Rangarajan, F. V. N., Fabian, A. C., Forman, W. R., Jones, C. 1995, MNRAS, 272, 665
Read, A. M., Ponman, T. J., & Strickland, D. K. 1997, MNRAS, 286, 626
Reeves, J. N., & Turner, M. J. L. 2000, MNRAS, 316, 234
Rice, W., Lonsdale, C. J., Soifer, B. T., Neugebauer, G., Koplan, E. L., Lloyd, L. A., de Jong, T., & Habing, H. J. 1988, ApJS, 68, 91
Sarazin, C. L., Irwin, J. A., & Bregman, J. N. 2000, ApJ, 544, L101 (SIB00)
Sarazin, C. L., Irwin, J. A., & Bregman, J. N. 2001, ApJ, 556, 533 (SIB01)
Schlegel, D. J., Finkbeiner, D. P., & Davis, M. 1998, ApJ, 500, 525
Shirey, R., et al. 2001, A&A, 365, L195
Terlevich, R., Davies, R. L., Faber, S. M., & Burstein, D. 1981, MNRAS, 196, 381
Trinchieri, G., Fabbiano, G., & Canizares, C. R. 1986, ApJ, 310, 637
Tonry, J. L., Dressler, A., Blakeslee, J. P., Ajhar, E. A., Fletcher, A. B., Luppino, G. A.,, Metzger, M. R., & Moore, C. B. 2001, ApJ, 546, 681
van Driel, W., Rots, A. H., & van Woerden, H. 1988, A&A, 204, 39
van Driel, H. & van Woerden, H. 1991, A&A, 243, 71